Supporting information for "Elasto-Inertial Instability in Torsional Flows of Shear-Thinning Viscoelastic Fluids"

Rishabh V. More[1]†, R. Patterson[2], E. Pashkovski[2] and G. H. McKinley[1]

[1]Department of Mechanical Engineering, Massachusetts Institute of Technology, Cambridge, MA 02139, USA

[2]The Lubrizol Corporation, 29400 Lakeland Blvd., Wickliffe, OH 44092, USA

(Received xx; revised xx; accepted xx)

This file of supporting information contains a full rheological characterization of the various PIB solutions used in this study and is provided for researchers interested in performing detailed numerical simulations or linear stability analysis of the inertio-elastic torsional flow instability presented in this work.

We prepared four different PIB solutions by varying the concentration of the PIB solute. Decreasing the PIB concentration lowers the viscoelasticity, decreases the extent of shear-thinning in the solutions, and reduces the first normal stress difference generated in strong, steady shearing flows.

Key words: Cross model, Generalized Rouse-Zimm Model, Relaxation time

---

1. Material and rheological properties of the fluids

In table 1, we summarize some material properties for the family of polymeric fluids used in the study. These values are primarily set by the GADDTAC solvent rather than the small amounts of high molecular weight polyisobutylene (PIB) polymer. Table 2 summarizes the best-fit parameters for the Cross shear-thinning model

$$\eta(\dot{\gamma}) = \eta_\infty + \frac{\eta_0 - \eta_\infty}{[1 + (\lambda\dot{\gamma})^n]} \tag{1.1}$$

obtained by regression to the stable steady-state shear viscosity data presented in Figure 1a of the main text. Here λ has the units of time and can also be written as a characteristic shear rate $\dot{\gamma}^* = \lambda^{-1}$. These fits to the Cross model are used to calculate the evolution in the shear thinning parameter $\beta_P(\dot{\gamma}; c_P) = (\eta(\dot{\gamma}; c_P) - \eta_\infty(c_P))/\eta(\dot{\gamma}; c_P)$ for each fluid composition. The extent of shear-thinning can also be clearly visualized in terms of the difference between the zero and the infinite shear rate limiting values of the viscosity, viz., η_0 and η_∞, respectively, as shown in Fig. S1. As the concentration exceeds the critical overlap concentration c^* and the solutions become semi-dilute, the zero-shear-rate viscosity increases rapidly.

In Fig. S2, we show the viscoelastic responses measured in small amplitude oscillatory shear (SAOS) flow experiments using a concentric cylinder geometry for the various PIB solutions used in this study. We perform time-Temperature superposition (tTS) to construct master curves of the storage and loss moduli as functions of the reduced oscillation frequency $\omega_r = a_T\omega$,

† Email address for correspondence: morer@mit.edu

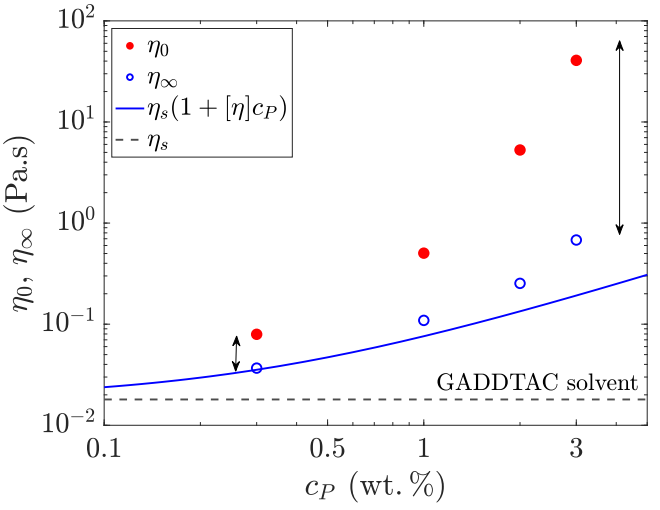

Figure S1: Variation in the zero-shear-rate viscosity η_0 and the infinite shear rate limiting value η_∞ obtained from the Cross model fit in Table 2 with increasing polymer concentration c_P. Also shown is the prediction of dilute solution theory (Kraemer 1938; Bird *et al.* 1987) given by $\eta_0 = \eta_s(1 + k_M[\eta]c_P)$ (solid line) obtained using the intrinsic viscosity $[\eta]$ of the PIB polymer for comparison. We note that because we are considering semi-dilute polymer solutions $\eta_\infty \neq \eta_s$, i.e., the presence of the polymer solute increases the shear viscosity of the polymer solutions even at very high shear rates. However, because $\eta_0(c_P) \gg \eta_\infty$, the difference between $\eta_0 - \eta_\infty$ and $\eta_0 - \eta_s$ is negligible.

c_P (wt. %)	ρ (kg/m^3)	Γ (mN/m)	η_s (Pa.s)	$[\eta]$ (dL/g)	c^* (wt. %)
0.30 – 3.00	873.1	29.7	0.018	3.69	0.23

Table 1: PIB polymer solution properties.

c_P (wt. %)	η_0 (Pa.s)	η_∞ (Pa.s)	λ (s)	n
3.0	40.7	0.68	6.19	0.72
2.0	5.28	0.25	1.20	0.62
1.0	0.50	0.11	0.12	0.71
0.3	0.10	0.05	0.06	0.81

Table 2: Best fit parameters for the Cross model Eq. 1.1 for the stable, steady-state rate-dependent shear viscosity data (Figure 1a in the main text) of various PIB solutions used in this study.

denoted $G'(\omega_r)$ and $G''(\omega_r)$, respectively. This allows us to extend the range of measurements to sufficiently low frequencies to observe the scaling expected in the terminal regime. Here ω is the oscillatory frequency, and a_T is the temperature-dependent horizontal shift factor. For the limited range of temperatures 10 °C $\leq T \leq$ 80 °C studied here, we find the vertical shift factor $b_T \approx 1$ for these PIB solutions, and there is no need to shift the $G'(\omega_r)$ and $G''(\omega_r)$ data vertically. In addition, we observe that even though the solutions are in the semi-dilute regime, the generalized

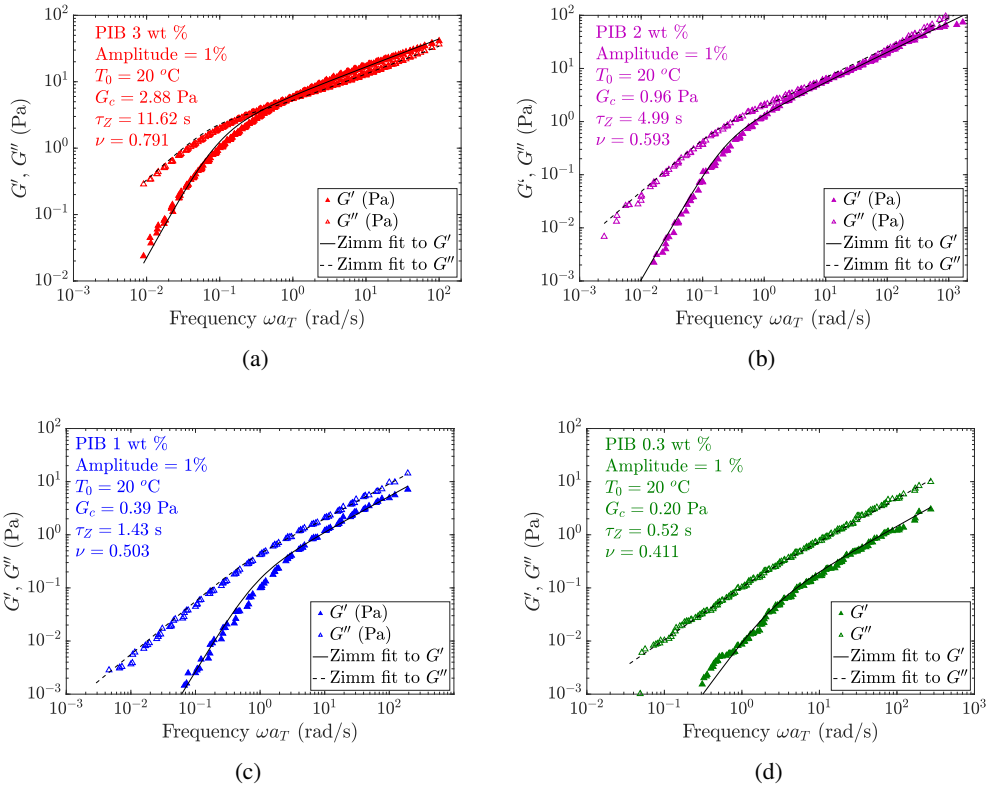

Figure S2: Small Amplitude Oscillatory Shear test data at a strain amplitude $\gamma_0 = 1$ % for the four PIB solutions utilized in this study and the corresponding generalized Rouse-Zimm model fits with the best-fit model parameters given in Table 3. (a) 3 wt. %. (b) 2 wt. %, (c) 1 wt. %, and (d) 0.3 wt. %. Time-temperature superposition using a reference temperature $T_0 = 20$ °C is employed to construct a master curve with a lateral shift factor a_T giving the reduced frequency $\omega_r = a_T\omega$. The generalized Rouse-Zimm model (Eq. 1.2) does an excellent job of fitting the SAOS data, and the corresponding fits are shown using black lines.

Rouse-Zimm model expressed in the form (Rubinstein & Colby 2003)

$$G'(\omega_r) = G_c \frac{\omega_r\tau_Z \sin\left[\chi \text{atan}(\omega_r\tau_Z)\right]}{\left[(1+(\omega_r\tau_Z)^2)\right]^{\chi/2}}, \tag{1.2a}$$

$$G''(\omega_r) = G_c \frac{\omega_r\tau_Z \cos\left[\chi \text{atan}(\omega_r\tau_Z)\right]}{\left[(1+(\omega_r\tau_Z)^2)\right]^{\chi/2}} \tag{1.2b}$$

does a good job of fitting the SAOS data, as shown in Fig. S2 by solid and dashed lines. Here, the fitting parameters are the characteristic modulus G_c, the Zimm relaxation time τ_Z, and $\chi = (1 - 1/3\nu)$ with ν being the solvent quality exponent. The best-fit parameter values for the generalized Rouse-Zimm model are tabulated in Table 3.

We can now use the best fits of the generalized Rouse-Zimm model to evaluate the value of the characteristic relaxation time in a shear flow, which is defined as $\tau_s = \lim_{\omega\to 0} G'/(\omega G'')$ (Bird *et al.* 1987; Arnolds *et al.* 2010). Using the generalized Rouse-Zimm model (Eq. 1.2*a*) we obtain,

$$\tau_s = \lim_{\omega\to 0} G'/(\omega G'') = \chi\,\tau_Z. \tag{1.3}$$

The values of τ_s thus obtained from this procedure are tabulated in Table 3 and used in the

c_P (wt. %)	G_c (Pa)	τ_Z (s)	χ	ν	τ_s (s)	η_0 (Pa.s)	El_0
3.00	2.88	11.62	0.579	0.791	6.73	40.7	783
2.00	0.96	4.99	0.438	0.593	2.19	5.28	33
1.00	0.39	1.43	0.337	0.503	0.48	0.50	0.69
0.30	0.20	0.52	0.189	0.411	0.10	0.10	0.02

Table 3: Generalized Rouse-Zimm model fit parameters for the linear viscoelastic properties obtained from master curves of the small amplitude oscillatory shear (SAOS) flow data for various PIB solutions obtained using a concentric cylinders geometry, as well as the shear relaxation time τ_s, which gives the first normal stress difference coefficient $\Psi_{1,0} = 2\eta_P\tau_s$. Also tabulated are the elasticity numbers for (hypothetical) second-order fluids with constant viscosities of η_0 and relaxation times of τ_s in a geometry with a characteristic radius of 20 mm. These values of El_0 are used in constructing Figure 4a of the main text (dashed lines).

main text to calculate the Deborah number De_0 and the Weissenberg number Wi_0 of the PIB solutions before shear-thinning is incorporated. Importantly, we see that for a 10-fold variation in concentration, we obtain an approximately 10-fold increase in the modulus G_c, but a much larger increase in both τ_z (or τ_s) and η_0.

2. First normal stress difference and the effects of shear-thinning on the Weissenberg number of the flow

From the functional form of the upper-convected derivative, the first normal stress difference can be described as $N_1(\dot\gamma) \simeq 2\tau_s\dot\gamma\sigma$ (Bird *et al.* 1987), which after a slight rearrangement gives $S_R = N_1(\dot\gamma)/\sigma(\dot\gamma) \simeq 2\tau_s\dot\gamma$. This ratio of N_1 to σ is termed the *stress ratio* in the main text and serves as a direct quantitative measure of non-linear viscoelastic effects in these polymeric solutions (see Figure 1b in the main text). One can also eliminate $\dot\gamma$ by substituting $\dot\gamma = \sigma/\eta$, which gives $N_1 \sim 2(\tau_s/\eta)\sigma^2$. So, one can expect N_1 to vary quadratically with σ. Furthermore, τ_s and η are both functions of the polymer concentration c_P and increase rapidly for larger dissolved polymer concentration, as seen in Table 3. As a result, the ratio $G_c(c_P) \sim \eta(c_P)/\tau_s(c_P)$ (Bird *et al.* 1987) only increases weakly with increasing the polymer concentration c_P, which can also be seen from the values of G_c in Table 3. Hence, $N_1 \sim 2(\tau_s/\eta)\sigma^2 \sim \sigma^2/G_c(c_P)$ is expected to decrease weakly with the polymer concentration c_P in the fluids utilized and we plot the first normal stress difference N_1 as a function of the shear stress σ in Figure S3a (same as Fig. 1c in the main manuscript, reproduced here for completeness) to test this prediction. We find that not only $N_1 \sim \sigma^2$, but this relationship also holds irrespective of the polymer concentration except when the flow becomes unsteady (hollow symbols). Thus, we can potentially estimate the steady state values of $N_1(\dot\gamma)$ from the measurements of steady-state shear stress alone. This can be an effective way of estimating N_1 in semi-dilute solutions because measuring N_1 is typically challenging owing to the sensitivity limitations of normal force transducers in commercial rheometers. For example, the state-of-the-art ARES-G2 rheometer (TA instruments) has a practical lower sensitivity limit of 0.001 N (0.1 gm-force) for the axial force F_{CP}, which gives a minimum value for the first normal stress difference $N_1 = 2F_{CP}/(\pi R^2)$ in a cone-plate geometry with radius R. So, a 40 mm cone-plate geometry, for instance, will not be sensitive to a first normal stress difference below approximately $N_1 \lessapprox 1.6$ Pa.

In addition, Laun's rule (Laun 1986) is an empirical relationship that allows the estimation of the first normal stress difference N_1 for highly viscoelastic fluids such as entangled polymer melts using small amplitude oscillatory shear measurements. In Figure S3b, we present a comparison

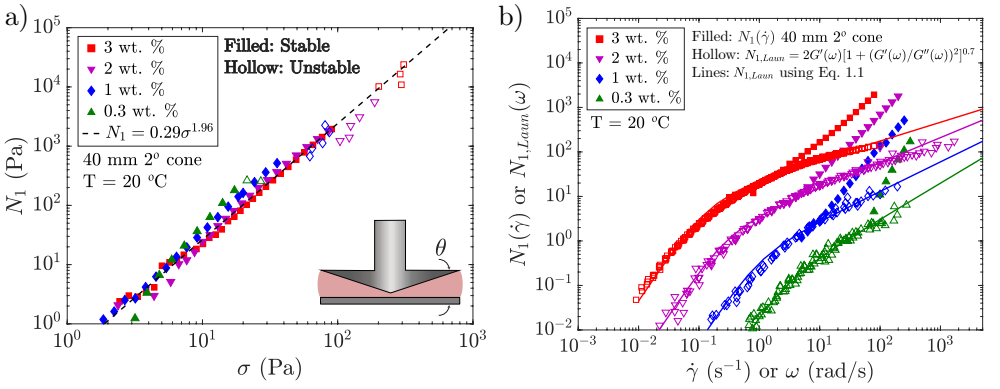

Figure S3: a) The first normal stress difference N_1 plotted as a function of the shear stress σ for all the PIB solutions used in this study in a 40 mm 2° geometry. The data lies almost on a single curve irrespective of the polymer concentration in solution with a power law best fit given by $N_1 \sim \sigma^{1.96}$, which is very close to the expected quadratic dependence of N_1 on σ. b) Comparison of the steady shear N_1 measurements in a 40 mm 2° cone-plate geometry with the predictions of Laun's Rule, $N_{1,Laun} = 2G'(\omega)[1+(G'(\omega)/G''(\omega))^2]^{0.7}$ (Laun 1986), which provides a way to estimate normal stress difference from small amplitude oscillatory shear measurements. Laun's rule does a decent job at predicting N_1 in the low and intermediate shear rate regimes, while it deviates away from the actual steady-shear measurements of N_1 at high shear rates.

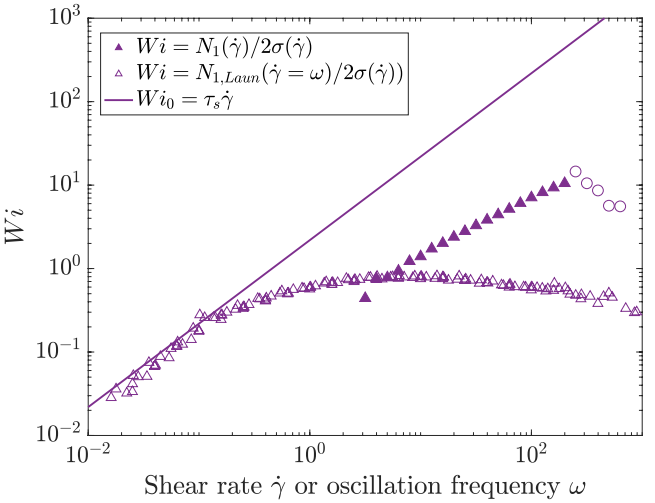

Figure S4: Comparison between non-shear-thinning Weissenberg number $Wi_0 = \lambda\dot{\gamma}$ (solid line) and shear-thinning Weissenberg number $Wi = N_1/2\sigma$ (filled triangle symbols) in the high shear-rate regime and $Wi = N_{1,Laun}/2\sigma$ in the low and intermediate shear rate regimes (hollow triangle symbols) for the 2 wt. % solution. Hollow circle symbols depict unstable flow conditions. The effect of shear-thinning in the relaxation time leads to a reduction in the rate of increase in the Weissenberg number Wi with increasing shear rate as opposed to a linear increase in the case of a constant relaxation time, e.g., Boger fluids.

of Laun's rule prediction for the first normal stress difference $N_{1,Laun}(\dot{\gamma})|_{\dot{\gamma}=\omega} \simeq 2G'(\omega)[1 + (G'(\omega)/G''(\omega))^2]^{0.7}$ using the small amplitude oscillatory shear and the corresponding generalized Rouse-Zimm model fits from Figure S2 and Table 3. Laun's rule estimates for the magnitude of $N_1(\dot{\gamma})$ in the low and intermediate shear rate regimes agree well with the steady shear values of N_1; however, they underpredict the actual measurements of $N_1(\dot{\gamma})$ in steady, simple shear flow at high shear rates.

The consequences of this complex shear-rate dependence of the first normal stress difference for semi-dilute polymer solutions are presented in Fig. S4. Here, we show a comparison of a rate-independent estimate of the Weissenberg number $Wi_0 = \tau_s\dot{\gamma}$ (solid line), where τ_s is obtained from linear viscoelastic measurements (Eq. 1.3) and assumes a constant rate-independent characteristic time, with a rate-dependent Weissenberg number Wi calculated using the general definition $Wi = N_1/2\sigma$ (White 1964) based on the data depicted in Fig. S3a in the high shear-rate regime and $N_{1,Laun}(\dot{\gamma})|_{\dot{\gamma}=\omega} \simeq 2G'(\omega)[1 + (G'(\omega)/G''(\omega))^2]^{0.7}$ using the small amplitude oscillatory shear in the low and intermediate shear-rate regimes based on the data depicted in Fig. S3b. When employing a constant relaxation time, one anticipates a linear rise in Wi_0 with shear rate. However, shear-thinning behavior introduces a relaxation time that decreases with increasing shear rate (see Eq. 2.3 in the main manuscript). Consequently, in the case of pronounced shear-thinning, which is true for the 3 wt. % and 2 wt. % fluids, the relaxation time $\tau_s(\dot{\gamma})$ can decrease substantially with increasing shear rate $\dot{\gamma}$. Consequently, a properly defined rate-dependent Weissenberg number $Wi(\dot{\gamma}) = N_1(\dot{\gamma})/2\sigma(\dot{\gamma})$ may be substantially smaller than the rate-independent estimate Wi_0 at the critical shear rate $\dot{\gamma}_c$, as evidenced in Fig. S4.

REFERENCES

Arnolds, Oliver, Buggisch, Hans, Sachsenheimer, Dirk & Willenbacher, Norbert 2010 Capillary breakup extensional rheometry (CaBER) on semi-dilute and concentrated polyethylene oxide (PEO) solutions. *Rheologica Acta* **49**, 1207–1217.

Bird, Robert Byron, Armstrong, Robert Calvin & Hassager, Ole 1987 *Dynamics of Polymeric Liquids. Vol. 1: Fluid Mechanics*. John Wiley and Sons Inc., New York, NY.

Kraemer, Elmer O 1938 Molecular weights of celluloses and cellulose derivates. *Industrial & Engineering Chemistry* **30** (10), 1200–1203.

Laun, HM 1986 Prediction of elastic strains of polymer melts in shear and elongation. *Journal of Rheology* **30** (3), 459–501.

Rubinstein, Michael & Colby, Ralph H 2003 *Polymer Physics*. Oxford University Press (New York).

White, James Lindsay 1964 Dynamics of viscoelastic fluids, melt fracture, and the rheology of fiber spinning. *Journal of Applied Polymer Science* **8** (5), 2339–2357.